Pramana – J. Phys., Vol. 38, No. 3, March 1992, pp. 291–312. © Printed in India.

Yields of evaporation residues and average angular momentum in heavy ion induced fusion reactions leading to compound nucleus ^{96}Ru

M DASGUPTA, A NAVIN*, Y K AGARWAL, C V K BABA, H C JAIN, M L JHINGAN and A ROY†

Tata Institute of Fundamental Research, Bombay 400 005, India
*Nuclear Physics Division, Bhabha Atomic Research Centre, Bombay 400 085, India
†Present address: Nuclear Science Centre, JNU New Campus, Post Box No. 10502, New Delhi 110 067, India

MS received 23 October 1991

Abstract. Cross-sections for production of evaporation residues from the compound nucleus ^{96}Ru* formed by fusion reactions ^{28}Si + ^{68}Zn, ^{32}S + ^{64}Ni, ^{37}Cl + ^{59}Co and ^{45}Sc + ^{51}V have been obtained from the yields of their characteristic γ-rays. The measurements span an excitation energy range of 55 MeV to 70 MeV of the compound nucleus. The evaporation residue (ER) cross-sections have been analysed in terms of statistical model for the decay of the compound nucleus. A good agreement is found between statistical model calculation and the experimental evaporation residue cross-sections in all the four cases. It is shown that the average angular momentum $\bar{\ell}$ of the compound nucleus can be deduced from a comparison of the experimentally measured and the statistical model predictions for the ER cross-sections. The validity of this method of deriving $\bar{\ell}$ has been discussed for the case of ^{16}O + ^{154}Sm system.

Keywords. Fusion reactions near Coulomb barrier; characteristic γ-ray measurements; evaporation residue cross-sections; statistical model; σ_{fusion}; average angular momenta.

PACS No. 25·70

1. Introduction

The study of heavy-ion fusion reactions is a topic of current interest (Signorini *et al* 1988). Such reactions are employed to produce nuclei at high excitation energies and angular momenta for nuclear structure studies. Apart from this, there is a considerable interest in trying to understand the mechanism of fusion reactions for a large range of energies and a variety of target-projectile combinations. The measured cross-sections for sub-barrier energies have been found to be orders of magnitude larger than those expected on the basis of simple one dimensional barrier penetration models (Beckerman 1988; Steadman and Rhoades–Brown 1986). While there is a good understanding of the process for relative kinetic energies of a few MeV per nucleon above the barrier, there are still unsolved problems for higher energies, especially in heavy systems (Mosel 1985). An associated problem of interest is connected with the decay of the nucleus formed after fusion. Evaporation residues (ERs) are formed after the fused system de-excites by particle emission. The mass distributions of the ERs have been studied in a few cases (Pühlhofer 1977). In some cases, the same compound nucleus (CN) formed at similar excitation energy and angular momentum, by different projectile-target combinations showed different relative ER populations, indicating

entrance channel effects (Ruckelshausen *et al* 1986). It has been reported that the energy spectra of the evaporated charged particles are *softer* (Alexander *et al* 1982) when compared to statistical model calculations. Thus it is necessary to study the formation and decay of CN systems in a number of cases and over wide excitation energy and angular momentum ranges. Such studies can lead to a better determination of the statistical model parameters. As is shown below, these models can then be used to derive other useful properties of the CN, like the average angular momentum.

The ER yields can be measured either by detecting ERs themselves through time-of-flight techniques and/or recoil mass analysers, or by detecting them by measuring the yields of their characteristic γ-rays. In the first method, the angular distribution of the ERs with respect to the beam direction, which comes about as a result of the transverse momentum imparted to them by the evaporating particles, has to be investigated in detail for obtaining the ER yields. In the recoil mass analysers, the charge state distribution of the ERs coming out of the target causes another source of uncertainty. The gamma-ray method requires a prior knowledge of the level schemes of the ERs, but is largely independent of the angular distributions of the recoiling ERs. In the medium mass region, specially near the Coulomb barrier, the total yield of residual nuclei can be taken as the total fusion yield as no other competing fusion-like reaction mechanism, like incomplete fusion are present.

In the present work the decay of the CN ^{96}Ru produced in the fusion reactions ^{28}Si + ^{68}Zn, ^{32}S + ^{64}Ni, ^{37}Cl + ^{59}Co and ^{45}Sc + ^{51}V has been studied using the γ-ray method. The measurements span an excitation energy range of 55 MeV to 70 MeV and an average angular momentum range of $6\hbar$ to $30\hbar$ in the CN. The yields of a large number of ERs from the decay of the ^{96}Ru compound nucleus have been measured and compared to the statistical model predictions. Having established the values of the statistical model parameters, data on the relative ER yields have been used to derive average angular momenta, $\bar{\ell}$, in the CN.

The experimental details of the present work and the results of the evaporation residue cross-section are given in § 2. A brief description of the statistical model and the parameters used is given in § 3. In § 4, a method is described whereby the average angular momentum can be derived from the relative yields of the ERs. The importance of average angular momenta, so obtained, in the fusion process has been discussed in an earlier report (Dasgupta *et al* 1991). Section 5 gives a summary and conclusions of the present work.

2. Experimental details

2.1 *Beams and targets*

The CN ^{96}Ru was produced in the present work through four different target projectile combinations. Table 1 shows details of these combinations and the energy ranges for which measurements were made. The experiments were performed at the Tata Institute of Fundamental Research (TIFR) – Bhabha Atomic Research Centre (BARC) pelletron accelerator facility, Bombay.

The momentum calibration of the analyzing magnet at the pelletron accelerator was made (Navin *et al* 1989) using the 14.231 MeV resonance in the ^{12}C(p,γ_0) ^{13}N (Ajzenberg–Selove 1986) reaction. The thickness of the targets used were such that

Table 1. Details of beams and targets.

Beam	Target	E_{lab} (MeV)	Current (pnA)	Target thickness ($\mu g/cm^2$)	Backing
^{28}Si	^{68}Zn (98·3% enriched)	70–100	5–15	146 ± 36, 123 ± 27	Bi
^{32}S	^{64}Ni (97·9% enriched)	78–100	5–15	$30{\cdot}1 \pm 4{\cdot}5$, 88 ± 10	Au
^{37}Cl	^{59}Co (natural)	88–115	5–15	165 ± 11 and 136 ± 12, 123 ± 16	Bi
^{45}Sc	^{51}V (natural)	110–134	2–10	67 ± 7	Au

the energy loss of the beam was 1 to 3 MeV. The effective energy in each case was determined from the known target thickness and the measured excitation function and the energy loss tables (Northcliffe and Schilling 1970). It is estimated to have uncertainty of ~ 100 keV. The beam charge was measured by calibrated commercial current integrators.

All the targets used in this work were made by the vacuum evaporation method. The targets were backed by catcher foils/backings to collect the recoiling ERs. Foils of high Z materials were used as backings. In the case of ^{59}Co and ^{68}Zn the target materials were evaporated on to Bi backings (~ 30 mg/cm^2), thick enough to stop both the recoiling nuclei and the beam. Bismuth backings were made by repeated evaporation of Bi (purity 99·9%) on to a 1 mm thick copper backing. The copper backing was provided to act as a heat sink during the irradiation. In the remaining cases, the targets were evaporated on to thin (~ 600 μgm/cm^2) gold backings. The beam and recoil nuclei go through the gold foil and are stopped in a thick (50 mg/cm^2) gold catcher placed immediately after the target. Target thicknesses were determined using the X-ray fluorescence technique or proton induced X-ray emission (PIXE) method (in the ^{64}Ni case). In the X-ray fluorescence method, the 14·4 keV γ-ray from a ~ 25 mCi ^{57}Co source was used to produce the fluorescence. The target thicknesses were determined by comparing the characteristic X-ray yields from the target and a foil of known thickness (0·5 to 1·0 mg/cm^2 thick) of the same material in an identical geometry. Corrections were made for the absorption of the 14·4 keV γ-ray and the characteristic X-ray in the target. PIXE measurements were done using 2 MeV protons from the 5·5 MeV Van-de-Graff accelerator at BARC, Bombay. A Si(Li) detector with a resolution ~ 200 eV at 6·4 keV was used in both cases for measuring the X-rays. The typical uncertainties in the target thickness measurements were estimated to be ~ 10–15%.

2.2 *Measurements of γ-ray yields*

The gamma decays from ERs have been measured through on-line and off-line methods. The characteristic γ-ray energies and the half lives for the ERs are listed in table 2. In the on-line measurements, the γ-rays were detected by an energy and efficiency calibrated ~ 110 cm^3 HPGe detector, kept at a distance of $\simeq 5$ cm from the target at $\simeq 55°$ to the beam direction to minimize the angular distribution effects. To

Table 2. Characteristics of the measured evaporation residues (ER). $T_{1/2}$ and E_γ represent the half-life and characteristic γ-ray energy of ERs. The fraction of γ-ray yield per decay of the ERs is given in the last column. The values for $T_{1/2}$, E_γ and fractions have been taken from compilations by Lederer and Shirley (1978).

ER	Channel	Measurements	$T_{1/2}$	E_γ(keV)	Fraction (%)
^{94}Ru	$2n$	Off-line	52 min	367·2	79 ± 2
^{94}Tc	pn	Off-line	293 min	871·1	100
^{94m}Tc			52 min	871·1	94 ± 1
^{93}Ru	$3n$	On-line	—	1392	—
^{93}Tc	$p2n$	Off-line	2·7 hrs	1363·0	66 ± 2
^{93m}Tm			43 min	392·6	60 ± 2
^{93m}Mo	$2pn$	Off-line	6·9 hrs	684·7	$99·7 \pm 1·0$
				263·1	$56·7 \pm 5·0$
^{92}Ru	$4n$	Off-line	3·65 min	213·7	$91·7 \pm 0·2$
^{92}Tc	$p3n$	Off-line	4·4 min	1509·6	100
				773·0	97 ± 5
^{92}Mo	$2p2n$	On-line	—	1509·6	—
^{91}Mo	αn	On-line	—	1413·9	—
^{90}Mo	$\alpha 2n$	Off-line	5·7 hrs	257·3	$77·6 \pm 3·0$
				122·3	$64·1 \pm 3·7$
^{90}Nb	αpn	Off-line	14·6 hrs	1129·2	$92·7 \pm 5·0$
^{89}Nb	$\alpha p2n$	Off-line	2·0 hrs	1627·2	$3·6 \pm 0·2$

determine the cross-sections of short-lived ERs, the decay spectra were recorded for 10 min in the on-line configuration immediately after switching off the beam. The off-line measurements for long-lived ERs were made in a close geometry by removing the target (when the target is deposited on thick Bi) or the catcher to a different location after each irradiation. A set of two targets was used in the case where the target was evaporated on to thick Bi backing. The decay spectra were recorded for typically 3–4 h and even longer in some cases.

The compound nucleus ^{96}Ru was produced at similar excitation energy for all the cases studied in the present work. Though as many as 12 ERs have been identified, not all of them have been used for determination of total cross-sections as explained below. The yields of stable ERs, measured by on-line techniques, are obtainable from the sum of yields of all the transitions feeding the ground state plus the yield to the ground state itself, which cannot be determined by this method. The average angular momentum for all the cases measured in the present work at most of the measured energies is $\geqslant 12\,\hbar$. Thus, for low values of the ground state spin (e.g. 0^+ in the case of even–even ERs), it is a very good approximation to neglect the direct feed to the ground state. This approximation is in agreement with the yields of $(1/2)^-$ and $(13/2)^+$ activities of ^{93}Ru and $(2)^+$ and 7^+ activities of ^{94}Tc where the feed to the $(1/2)^-$ and $(2)^+$ state were measured to be less than 15% and 10% of that due to $(13/2)^+$ and 7^+ levels respectively. Further, in the case of an even–even nucleus (^{92}Mo for example), the $2^+ \rightarrow 0^+$ yield represents the total yield of the ERs to a good approximation. This was confirmed by measuring (Dasgupta *et al* 1988) the γ-ray yields following ^{92}Mo (α, 2n) ^{94}Ru. Thus for the even–even stable ERs the $2^+ \rightarrow 0^+$ γ intensity was taken to represent the total yield of the ERs. In some cases, the ground state spin of the stable ER is reasonably large, e.g., for the $3n$ channel resulting in ^{93}Ru, the ground state spin is $(9/2)^+$ (Lederer and Shirley 1978). In this case the measured

Table 3. Experimental evaporation residue (ER) cross-sections [in mb], fusion cross-sections, σ_{fus}, and deduced average angular momenta, $\bar{\ell}$, for the system $^{28}Si + ^{68}Zn$. $\Sigma_i \sigma_{ERi}$ represents the sum of the ER cross-sections given in columns (ii) to (ix). $f_{CASCADE}$ denotes the CASCADE predictions for the fraction of the total yield for these channels. The total fusion cross-section, σ_{fus}, unless mentioned otherwise, is obtained by dividing the values given for $\Sigma_i \sigma_{ERi}$ by $f_{CASCADE}$. The last column gives the value of $\bar{\ell}$ as described in the text. Uncertainties in the cross-section measurements, quoted within brackets, do not include the uncertainties due to target thickness. The uncertainty (within brackets) in the $\bar{\ell}$ values does not include the uncertainties due to analyses procedure (see text).

	Residual nucleus (exit channel)											
E_{CM} (MeV)	^{94}Ru ($2n$)	^{93}Tc ($p2n$)	^{92}Ru $4n$	^{92}Tc ($p3n$)	^{92}Tc + ^{92}Mo ($p3n + 2p2n$)	^{90}Mo ($\alpha 2n$)	^{90}Nb (αpn)	^{89}Nb ($\alpha p2n$)	$\Sigma_i \sigma_{ERi}$ (mb)	$f_{CASCADE}$	σ_{fus} (mb)	$\bar{\ell}$ ($\hbar$)
50·7[a]	—	0·34(0·04)	—	—	< 0·03	0·02(0·01)	—	—	0·36(0·05)	0·55[c](0·10)	0·62(0·13)	—
52·2[b]	0·01(0·01)	1·5(0·10)	—	—	0·50(0·20)	0·25(0·04)	0·30(0·06)	—	2·56(0·24)	0·72(0·06)	3·6(0·5)	< 6
53·6[a]	0·07(0·01)	13·0(0·50)	—	1·0(0·3)	3·6(0·2)	1·9(0·1)	1·9(0·2)	—	21·5(0·7)	0·75(0·05)	29(2)	6·6(0·8)
55·0[b]	0·13(0·02)	24·8(1·0)	—	2·9(0·3)	8·8(0·2)	4·6(0·1)	4·4(0·5)	—	43(1)	0·76(0·05)	56(4)	11·4(0·5)
56·4[a]	0·27(0·03)	31·8(1·1)	—	7·9(1·0)	16·1(0·5)	7·8(0·3)	5·7(0·7)	< 0·11	62(1)	0·78(0·04)	79(4)	12·4(0·4)
57·1[a]	0·33(0·02)	48·9(1·7)	—	12·4(0·6)	22·6(0·9)	11·6(0·4)	10·5(1·0)	2·3(0·7)	96(2)	0·79(0·04)	114[†](8)	14·8[†](0·4)
57·1[b]	0·36(0·04)	44·4(1·5)	—	9·0(0·4)	20·8(0·5)	9·5(0·3)	8·0(1·2)	1·3(0·5)	84(2)			
58·6[a]	0·43(0·04)	63·0(2·0)	—	17·2(0·6)	40·2(0·4)	16·0(0·5)	13·2(1·5)	4·5(1·7)	137(3)	0·80(0·04)	171(9)	15·8(0·4)
60·0[b]	0·52(0·06)	65(2)	—	25·4(0·7)	47·5(0·6)	20·0(0·7)	15·6(1·9)	8·2(1·4)	157(3)	0·81(0·04)	194(10)	17·5(0·4)
61·4[a]	0·68(0·06)	74(3)	—	35·9(0·9)	62·2(0·6)	23·8(0·8)	18·4(2·7)	13·2(2·2)	192(5)	0·82(0·04)	234(13)	18·5(0·8)
63·6[b]	0·62(0·06)	73(3)	1·5(0·8)	44(2)	82(2)	24·9(0·9)	13·8(4·7)	18·7(3·9)	214(7)	0·81(0·04)	264(16)	19·3(0·4)
65·7[a]	0·86(0·14)	97(4)	1·8(0·4)	61(2)	113(2)	42·2(1·4)	35(6)	55(4)	345(9)	0·80(0·04)	431(24)	21·4(0·3)
70·7[a]	1·1(0·3)	93(7)	4·6(0·7)	110(4)	131(5)	48(2)	47(14)	138(14)	463(22)	0·77(0·05)	572[†](38)	26·4[†](0·7)
70·7[b]	0·63(0·05)	81(4)	3·1(0·1)	86(3)	112(2)	47(2)	64(12)	114(15)	422(20)			

[a] ^{68}Zn target-thickness $(146 \pm 36)\mu g/cm^2$; [b] ^{68}Zn target-thickness $(123 \pm 27)\mu g/cm^2$; [†]Weighted average; [c]Only $p2n$ channel.

Table 4. Same as table 3 but for the case of $^{32}S + ^{64}Ni$. $\Sigma_i \sigma_{ER_i}$ is the sum of the ER cross-sections given in columns (iii) to (viii).

		Residual nucleus (exit channel)									
E_{LAB} (MeV)	E_{CM} (MeV)	^{93}Tc ($p2n$)	^{92}Tc ($p3n$)	$^{92}Tc + ^{92}Mo$ ($p3n + 2p2n$)	^{90}Mo ($\alpha 2n$)	^{90}Nb (αpn)	^{89}Nb ($\alpha p2n$)	$\Sigma_i \sigma_{ER_i}$ (mb)	$f_{CASCADE}$	σ_{fus} (mb)	$\bar{\ell}$ ($\hbar$)
78·6[a]	52·4	0·04(0·01)	—	0·02(0·01)	0·04(0·02)	0·04(0·02)	—	0·14(0·03)	0·71(0·06)	0·20(0·05)	—
80·8[b]	53·9	0·55(0·08)	—	0·12(0·08)	0·30(0·20)	0·20(0·60)	—	1·17(0·64)	0·74(0·05)	1·6(0·9)	—
82·7[a]	55·1	2·6(0·1)	0·5(0·2)	1·4(0·2)	0·35(0·02)	0·63(0·07)	—	4·98(0·24)	0·76(0·05)	6·6(0·5)	—
85·3[b]	56·9	9·8(0·9)	—	4·8(1·0)	2·2(0·4)	2·7(0·8)	—	19·5(1·6)	0·78(0·05)	25(3)	9·0(3·0)
86·7[a]	57·8	15·7(0·8)	4·3(0·8)	10·8(0·7)	3·3(0·1)	4·2(0·2)	0·7(0·3)	35(1)	0·81(0·05)	43(3)	9·9(1·0)
87·3[a]	58·2	19·7(1·1)	—	14·1(1·0)	3·9(0·2)	7·3(0·8)	0·8(0·6)	46(2)	0·81(0·04)	57(4)	10·8(0·8)
89·8[b]	59·9	30·0(2·0)	—	28·8(1·8)	2·3(0·3)	3·7(0·7)	—	65(3)	0·83(0·04)	78(5)	12·4(0·6)
92·1[a]	61·4	40·7(2·1)	21·8(1·4)	50·0(3·1)	10·9(0·4)	15·5(0·7)	11·5(4·1)	129(6)	0·84(0·04)	154(10)	14·2(0·6)
94·8[b]	63·2	60(3)	—	84(5)	20·0(2·0)	22·0(1·0)	11·0(5·0)	197(8)	0·84(0·04)	234(15)	16·0(0·6)
97·2[a]	64·8	61(3)	65(4)	113(7)	20·4(1·4)	31·7(1·3)	26·5(4·1)	253(9)	0·84(0·04)	301(18)	16·5(0·5)
99·8[b]	66·5	57(4)	—	99(7)	23·0(2·0)	30·0(2·0)	59(7)	268(11)	0·82(0·04)	327(21)	18·5(0·7)
104·7[a]	69·8	71(4)	96(5)	173(10)	33·0(2·0)	52(2)	78(8)	407(14)	0·80(0·05)	509(36)	19·6(0·6)
109·8[b]	73·1	66(5)	—	179(10)	36·0(5·0)	65(5)	192(20)	538(24)	0·78(0·04)	690(47)	23·0(1·0)

[a] ^{64}Ni target-thickness $(88 \pm 10)\mu g/cm^2$; [b] ^{64}Ni target-thickness $(30{\cdot}1 \pm 4{\cdot}5)\mu g/cm^2$.

Table 5. Same as table 3 but for $^{37}Cl + ^{59}Co$ system. $\Sigma_i \sigma_{ER_i}$ represents the sum of the ER cross-sections given in columns (iii) to (ix).

		Residual nucleus (exit channel)										
E_{LAB} (MeV)	E_{CM} (MeV)	^{94}Ru ($2n$)	^{93}Tc ($p2n$)	^{92}Tc ($p3n$)	$^{92}Tc + ^{92}Mo$ ($p3n + 2p2n$)	^{90}Mo ($\alpha 2n$)	^{90}Nb (αpn)	^{89}Nb ($\alpha p2n$)	$\Sigma_i \sigma_{ER_i}$ (mb)	$f_{CASCADE}$	σ_{fus} (mb)	$\bar{\ell}$ ($\hbar$)
90·1[a]	55·4	< 0·02	0·3(0·2)	—	—	1·8(1·4)	—	—	2·1(1·4)	0·60(0·08)[f]	0·5(0·3)	—
91·5[a]	56·2	< 0·02	0·8(0·2)	0·06(0·04)	0·24(0·03)	0·4(0·5)	—	—	1·4(0·5)	0·75(0·05)	1·9(0·7)	6·6(1·2)
93·0[a]	57·2	< 0·01	3·1(0·3)	0·67(0·10)	1·9(0·1)	0·7(0·6)	—	—	5·7(0·7)	0·78(0·05)	7·3(1·0)	< 6
93·0[b]	57·2	—	6·1(0·5)	—	4·0(0·4)	1·1(0·2)	1·5(0·4)	—	12·7(0·8)	0·78(0·05)	—	< 6
94·5[a]	58·1	< 0·01	8·4(0·9)	1·7(0·1)	4·9(0·2)	1·3(0·5)	2·2(1·0)	—	16·8(1·4)	0·79(0·04)	21(2)	8·9(1·4)
96·0[b]	59·0	—	24·9(0·2)	—	19·7(1·3)	6·3(0·5)	6·0(0·7)	—	57(2)		—	10·0(1·0)
97·6[a]	60·0	< 0·09	20·2(2·7)	7·4(0·5)	19·8(0·8)	—	12·4(6·2)	—	52(7)	0·77(0·05)[e]	68(2)	10·3(1·0)
98·6[a]	60·6	0·37(0·06)	32·2(1·2)	14·1(0·7)	31·6(1·7)	8·8(0·3)	8·5(1·0)	—	81(2)			
98·6[c]	60·6	0·14(0·07)	29·6(1·2)	12·2(0·6)	29·9(1·4)	8·4(0·4)	5·1(0·7)	—	73(2)	0·83(0·04)	100[†](5)	11·7[†](0·4)
98·6[d]	60·6	0·24(0·08)	35·2(1·3)	15·4(0·9)	35·3(1·6)	9·7(0·4)	8·4(0·7)	—	89(2)			
99·1[a]	60·9	< 0·2	31·8(2·1)	—	23·5(0·9)	8·2(2·0)	16·0(6·1)	< 1·2	80(7)	0·83(0·04)	96(10)	14·4(0·6)
101·6[a]	62·4	< 0·10	46·7(3·5)	26·9(1·0)	43·5(1·4)	8·2(2·4)	3·5(7·6)	4·1(1·0)	106(9)	0·84(0·03)	126(12)	15·7(0·6)
102·8[c]	63·2	0·6(0·2)	50·6(2·0)	31·2(1·4)	60·1(2·6)	16·0(0·7)	13·5(1·8)	11·0(4·2)	152(6)	0·84(0·03)	181(10)	15·6(0·3)
103·7[b]	63·7	—	83·1(6·0)	74·6(6·3)	120(6)	28·1(2·1)	31·6(1·0)	28·7(3·6)	292(10)		—	15·2(0·5)
104·0[a]	63·9	< 0·20	47·5(8·2)	25·8(1·4)	52·4(1·9)	15·0(4·9)	29(19)	45(22)	189(31)	0·84(0·03)	225(38)	17·0(0·7)
106·8[c]	65·6	0·4(0·1)	67·1(2·5)	49·3(2·0)	88·4(3·8)	24·6(1·2)	20·3(2·7)	16·7(4·4)	218(7)	0·84(0·03)	272[†](12)	18·0[†](0·7)
106·8[d]	65·6	0·6(0·2)	74·8(2·8)	58·1(2·4)	101(5)	27·9(1·0)	23·3(2·6)	27·2(4·5)	255(8)			
110·8[d]	68·1	1·1(3·0)	81·8(4·7)	73·9(3·2)	131(6)	34·6(1·3)	32·1(4·2)	35·2(5·9)	316(11)	0·84(0·03)	376(19)	19·3(0·5)
114·8[c]	70·6	1·5(0·4)	71·8(2·7)	76·7(3·4)	127(6)	34·2(1·2)	34·8(4·2)	63·8(6·7)	333(10)	0·84(0·03)	396(18)	21·2(0·4)

[a] ^{57}Co target-thickness $(165 \pm 11)\mu g/cm^2$; [b] Target-thickness $(136 \pm 12)\mu g/cm^2$; [c] ^{57}Co target-thickness $(123 \pm 16)\mu g/cm^2$; [d] Target thickness not determined; [e] Excluding $\alpha 2n$ channel; [f] Only $p2n$ channel; [†] Weighted average.

Table 6. Same as table 3 but for the case of $^{45}Sc + ^{51}V$ system. $\Sigma_i\sigma_{ER_i}$ represents the sum of the ER cross-sections given in columns (iii) to (viii). A ^{51}V target of thickness $(67 \pm 7)\mu g/cm^2$ was used during the measurements.

		Residual nucleus (exit channel)									
E_{LAB} (MeV)	E_{CM} (MeV)	^{93}Tc ($p2n$)	^{92}Tc ($p3n$)	$^{92}Tc + ^{92}Mo$ ($p3n + 2p2n$)	^{90}Mo ($\alpha 2n$)	^{90}Nb (αpn)	^{89}Nb ($\alpha p2n$)	$\Sigma_i\sigma_{ER_i}$ (mb)	$f_{CASCADE}$	σ_{fus} (mb)	$\bar{\ell}$ ($\hbar$)
109·7	58·3	0·14(0·02)	—	0·84(0·76)	—	—	—	0·98(0·76)	0·81(0·04)	1·20(0·90)	—
111·8	59·4	0·61(0·09)	0·13(0·07)	1·70(0·80)	0·42(0·09)	0·08(0·20)	1·10(0·80)	4·6(1·2)	0·84(0·03)	5·5(1·4)	< 9
114·8	61·0	2·9(0·1)	4·4(1·8)	7·2(0·5)	1·2(0·1)	0·9(0·3)	5·5(0·2)	17·7(0·6)	0·86(0·03)	20·6(1·0)	8·0(0·8)
117·8	62·6	7·5(0·5)	—	22·5(2·4)	3·1(1·3)	1·9(0·5)	6·6(2·2)	41·6(3·6)	0·87(0·03)	48(4)	10·2(0·8)
120·8	64·2	14·7(1·3)	—	37·1(5·0)	7·6(1·0)	8·0(3·0)	10·5(3·0)	78(7)	0·86(0·03)	91(9)	14·0(0·9)
124·0	65·9	17·4(1·6)	—	63(7)	8·9(1·3)	10·6(2·2)	18·0(6·0)	118(10)	0·85(0·03)	139(13)	14·1(0·8)
129·8	69·0	30·8(2·2)	—	105(9)	15·2(1·30)	15·8(3·0)	46(14)	213(17)	0·82(0·04)	260(24)	17·2(0·8)
133·8	71·1	41·3(7·3)	35(10)	117(18)	27·9(5·5)	24(11)	134(38)	344(44)	0·79(0·04)	435(60)	20·0(1·8)

yield of $(13/2)^+ \rightarrow (9/2)^+$ γ transition does not correctly represent the total yield of the ER. Such cases, even though analysed and corrected for angular momentum distribution, were not used in deriving the total fusion cross-section.

The partial cross-sections for the production for the various ERs have been determined from the measured γ-ray yields (after correcting for feedings from decay chains of neighbouring nuclei), known target thickness and the total number of beam particles incident on the target. While the relative cross-sections have uncertainties of ~ 5–7% due to counting statistics and the uncertainty in the determination of the detector efficiency, the absolute cross-sections have an additional uncertainty due to target thickness measurements. The partial cross-sections for the several channels so obtained are listed in tables 3–6, for the four different reactions. The errors quoted do not include the target thickness uncertainties.

3. Statistical model calculations

The statistical model code CASCADE (Pühlhofer 1977) was used to calculate the partial ER cross-sections. Only the decay and not the formation of the CN was considered. The statistical model analysis of the partial ER cross-sections has been performed with two separate objectives in mind. In the first part described in § 3.1, the ER cross-sections for several energies are compared with the predictions of the statistical model in order to determine the model parameters. In the second part, discussed in § 4, a more ambitious analysis is made in order to extract average angular momenta, $\bar{\ell}$, from the measured partial cross-sections.

In the statistical model, the emission probability for the decay of a CN at an excitation energy E_i and angular momentum J_i and parity π_i to a daughter nucleus f at an excitation energy between E_f and $E_f - dE_f$ and angular momentum J_f and parity π_f by the emission of a particle x with kinetic energy ε_x, spin s_x and orbital angular momentum ℓ, is given by (Thomas 1964),

$$R_x d\varepsilon_x = \frac{\Gamma_x(\varepsilon_x)}{\hbar} = \frac{\rho_f(E_f, J_f, \pi_f)}{2\pi\hbar\rho_i(E_i, J_i, \pi_i)} \sum_{S=|J_f - s_x|}^{J_f + s_x} \sum_{l=|J_i - S|}^{J_i + S} T_\ell(\varepsilon_x) d\varepsilon_x \tag{1}$$

where $\mathbf{S} = \mathbf{J}_f + \mathbf{s}_x$ is the channel spin in the exit channel and $E_i = E_f + \varepsilon_x + B_x$, B_x being the separation energy of x. ρ_i and ρ_f are the level densities in the parent and daughter nuclei respectively. The $T_\ell(\varepsilon_x)$ are the transmission coefficients in a time reversed reaction of the particle x of energy ε_x on the daughter nucleus f at an excitation energy E_f. One usually obtains these either from global optical model parametrization and/or from the scattering of x on the nucleus f in the ground state. Similarly the probability of decay by a γ-ray of energy between ε_γ and $\varepsilon_\gamma + \delta\varepsilon_\gamma$ and multipolarity λ to produce nuclei with energy between $E_f [E_i = E_f + \varepsilon_\gamma]$ and $E_f - dE_f$ and angular momentum J_f and parity π_f is (Sarantities and Pakes 1967; Grover and Gilat 1967)

$$R_\gamma d\varepsilon_\gamma = \frac{\Gamma_\gamma(\varepsilon_\gamma)}{\hbar} = \frac{\rho_f(E_f, J_f, \pi_f)}{2\pi\hbar\rho_i(E_i, J_i, \pi_i)} \zeta_\lambda(E_\gamma) \varepsilon_\gamma^{2\lambda+1} \tag{2}$$

$\zeta_\lambda(E_\gamma)$ are the energy dependent γ-ray strengths.

The code CASCADE follows such decays till the end (i.e. until no particle emission is energetically possible).

3.1 *Inputs*

The inputs to the program consist of (i) the ground state masses of the nuclei involved in the decay cascade (ii) the transmission coefficients for the inverse reaction involving the various emitted particles (iii) γ-ray strengths (iv) the level densities for the various nuclei as a function of excitation energy and angular momentum and (v) the angular momentum distribution in the CN. The above inputs are summarised in table 7 and are described briefly in the following:

(i) The ground state masses wherever experimentally known have been used (Wapstra and Bos 1977)

(ii) The emission of protons, neutrons and alpha has been considered. The optical potentials used for obtaining the transmission coefficient $T_\ell(\varepsilon_x)$ have been taken from the work of Perey (1963) for protons, from Wilmore and Hodgson (1964) for neutrons and from Huiezenga and Igo (1961) for alpha. All these potentials employ Woods–Saxon (WS) form for the radial dependence of both the real and imaginary parts. It was observed (Alexander *et al* 1982) that the charged particle spectra in general and alpha particle spectra in particular are softer than those expected on the basis of

Table 7. Parameters for the evaporation calculations using the code CASCADE.

Angular momentum distribution in the compound nucleus	As predicted by CCDEF
Optical potentials for emitted particles	
Neutrons	(Wilmore and Hodgson 1964)
Protons	(Perey 1963)
α particles	(Huizenga and Igo 1961) with two different diffuseness of 0·58 fm and 0·73 fm
γ-decay strengths	
E1 strength	10^{-4} W.u.
M1 strength	3×10^{-2} W.u.
E2 strength	5 W.u.
GDR energy	15·0 MeV
GDR width	5·5 MeV
GQR	No GQR
Level density parameters	
Region $I(E^* < 10\,\text{MeV})$	
Level density formula	Fermi gas level density
Moment of inertia	Effective moment of inertia $I_{\text{eff}} = 0{\cdot}62\, I_{\text{rigid}}$
Pairing energy	From ground state mass differences
Backshifting of the ground state	No backshifting
Region III ($E^* > 20\,\text{MeV}$)[a]	
Level density formula	Fermi gas level density[b]
Level density parameter	$A/9\,\text{MeV}^{-1}$
Moment of inertia	Rigid body with $r_0 = 1{\cdot}23$ fm
Deformation	Liquid drop theory
Deformability[c]	$b = 4{\cdot}7 \times 10^{-6}$; $c = 1{\cdot}2 \times 10^{-8}$

[a]The level density parameters are linearly extrapolated between regions I and III.
[b]The virtual ground state is calculated using a liquid drop ground state without shell and pairing.
[c]Used to calculate the effective moment of inertia $I_{\text{eff}} = I_{\text{sper}}\,(1 + b\ell^2 + c\ell^4)$.

statistical model calculation and it was conjectured that this may be due to a deformation in the CN. In order to investigate this point we made calculations with two different diffuseness parameter in the real part of the WS potential (0·58 fm and 0·73 fm) keeping the other parameters constant. The effects of this change in the diffuseness parameters will be discussed in the next section.

(iii) Gamma-decay: The giant electric dipole resonance with a strength of 100% EWSR and a uniform 5 Weisskopff units for E2 decay mode has been considered. The location of GDR resonance is taken as $78\,A^{-1/3}$. A Lorentzian form for the γ-strength $\zeta(E_\gamma)$ with a cut-off at 32 MeV has been used. A single particle strength for M1 decay was used in the calculations.

(iv) The level density is an important ingredient in the statistical model calculations. Following Dilg (1973) the expression used for the level density $\rho(E^*, J)$ has the form

$$\rho(E^*, J) = \frac{(2J+1)}{24\sqrt{2}\sigma^3 a^{(1/4)}} \frac{\exp[2\{a(E^*-\Delta)\}^{1/2} - J(J+1)/2\sigma^2]}{(E^*-\Delta+t)^{5/4}} \tag{3}$$

where a is the level density parameter and t is the thermodynamic temperature. The ground state correction, Δ, has two contributions. The correction due to pairing correlation and a backshift introduced by Dilg *et al* (1973). The pairing energies extracted from the ground state masses in the region $A \simeq 96$ were used in the calculations. σ is the spin cut-off parameter defined as $\sigma^2 = I_{\text{eff}} t/\hbar^2$ where I_{eff} is the effective moment of inertia. The moment of inertia parameter for angular momenta up to spins of 16 $\hbar$ was extracted from the known yrast levels of ^{92}Mo and ^{92}Ru. This corresponds to 0·62 of the moment of inertia of a rigid body. For higher angular momenta, a form $I_{\text{eff}} = I_{\text{sper}}(1 + b\ell^2 + c\ell^4)$ as suggested by Pülhofer (1977) was used.

(v) The angular momentum distribution in the CN has an important influence on the relative ER fractions. The experiments were performed at energies ~ 5 MeV below to 10 MeV above the Coulomb barrier. It is now widely known that in HI fusion reactions below the barrier, the fusion cross sections are often orders of magnitude higher than those calculated on the basis of one dimensional barrier penetration models (BPM). The angular momentum distributions are also found to be wider (extending to larger ℓ's) as compared to the expectations on the basis of BPM. Several models have been proposed to explain these features. It is seen that the simplified coupled channel calculations with inclusion of couplings to the inelastic channels give reasonable agreement with the experimentally measured average angular momentum (Beckerman 1988). Therefore, in the absence of information regarding the ℓ-distribution in the CN at sub-barrier energies, the predictions of the simplified coupled channel model (using the code CCDEF) (Fernández–Niello *et al* 1989) were used in the calculations. It is well known that ℓ-distribution in the CN at energies much above the barrier are well represented by,

$$\sigma_\ell(E) \propto \frac{2\ell+1}{[1+\exp\{(\ell-\ell_0(E))/a\}]}. \tag{4}$$

All the above mentioned [(i)–(v)] parameters in the code were fixed at energies above barrier by assuming a form given by (4) for the ℓ-distribution and then comparing the experimental values for the evaporation residue yields with those predicted by CASCADE. The CASCADE parameters obtained in the above manner,

together with the ℓ-distribution as given by the simplified coupled channel code CCDEF were utilized to calculate the relative ER yields at bombarding energies where the measurements were made. As described above, in the later calculations the ℓ-distributions as predicted by simplified coupled channel model code, were used.

3.2 *Comparison with experimental results and determination of total fusion cross-sections*

The relative evaporation residue cross-sections were calculated using the above parameters (see table 7) in CASCADE. The total cross-section could then be obtained by summing the cross-sections for the measured channels and then by dividing the sum by the summed fractions for these channels as given by CASCADE. For most of the systems studied in this work, evaporation channels $p2n$, $p3n$, $2p2n$, $\alpha 2n$, αnp, $\alpha 2np$ have been used for the determination of total fusion cross-sections. These channels exhaust 75–85% of the total cross-section in the region of interest. In order to check the reliability of the parameters used in CASCADE, the experimentally measured fractional cross-sections were compared to those predicted by CASCADE. A comparison of the experimental data with the CASCADE predictions are shown in figures 1–4 for all the four systems with the channels grouped according to the total number of particles emitted i.e. $p2n$, $(p3n + 2p2n)$, $(\alpha 2n + \alpha pn)$ and $\alpha p2n$. The set of CASCADE parameters used in the above calculations are summarized in table 7. A detailed comparison of the fractional yields for all the measured channels in case of $^{28}Si + {}^{68}Zn$ at excitation energies of 49·6 MeV and 56·0 MeV which correspond to centre of mass energies 0·7 MeV below and 6 MeV above the barrier is shown in figure 5. The experimentally measured values can be seen to agree fairly well with the CASCADE predictions. However, the CASCADE predictions for the $\alpha p2n$ channel are less than the experimentally observed values for all the four cases. This may be due to the level density in nuclei far removed from the CN (as in the case of $\alpha p2n$) not having been specified properly. The parameters used in the code were optimized for $A \sim 96$. It may be possible to obtain a better fit by slightly changing the pairing

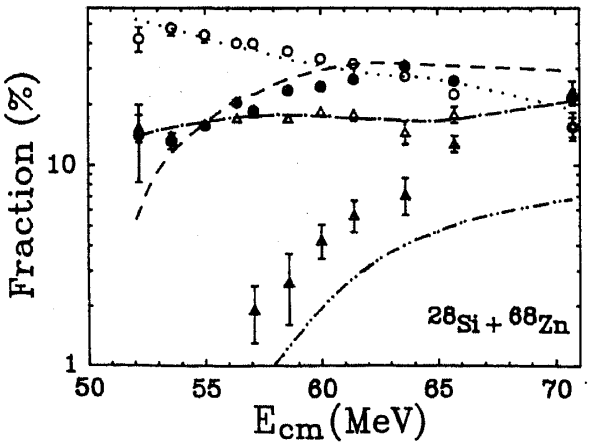

Figure 1. Comparison between measured and calculated fractional evaporation residue yields for $p2n$ (open circle, dotted curve), $p3n + 2p2n$ (filled circle, dashed curve), $\alpha 2n + \alpha pn$ (open triangle, dash-dot curve) and $\alpha p2n$ (filled triangles, dash-dot-dot curve) in fusion reactions of $^{28}Si + {}^{68}Zn$. The calculations were performed using the statistical model code CASCADE (see text).

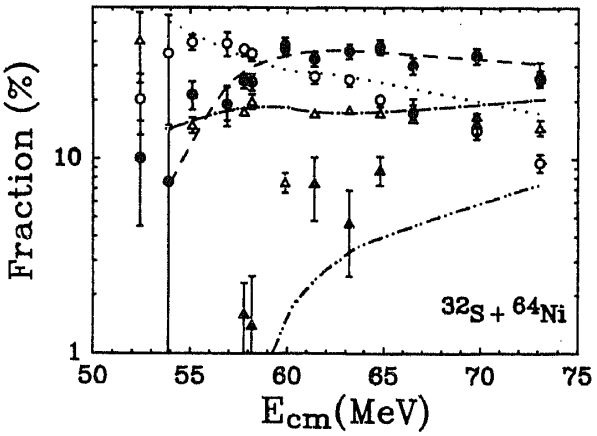

Figure 2. Comparison between measured and calculated fractional evaporation residue yields for fusion reaction of $^{32}S + ^{64}Ni$. See caption of figure 1 for explanation.

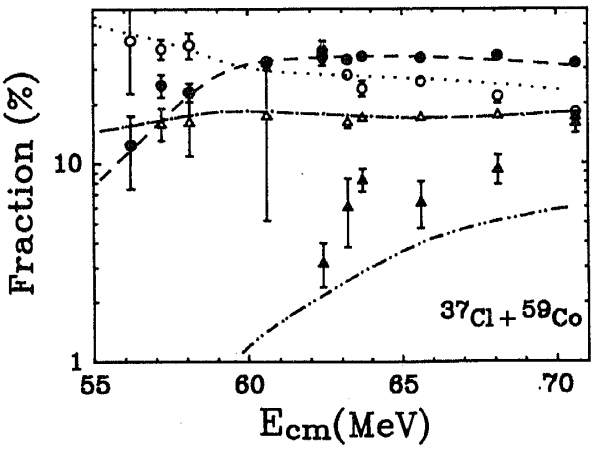

Figure 3. Comparison between measured and calculated fractional evaporation residue yields for fusion reaction of $^{37}Cl + ^{59}Co$. See caption of figure 1 for explanation.

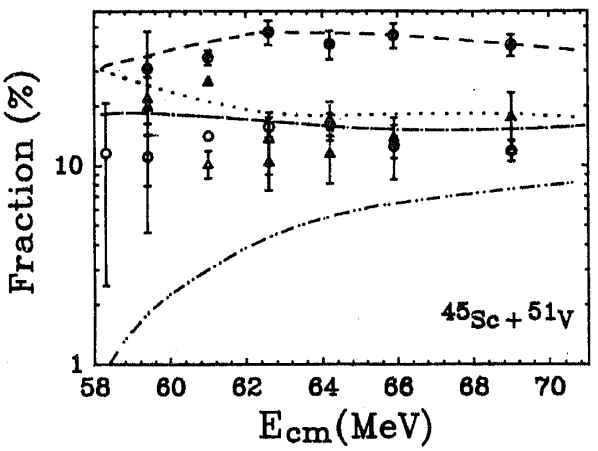

Figure 4. Comparison between measured and calculated fractional evaporation residue yields for fusion reaction of $^{45}Sc + ^{51}V$. See caption of figure 1 for explanation.

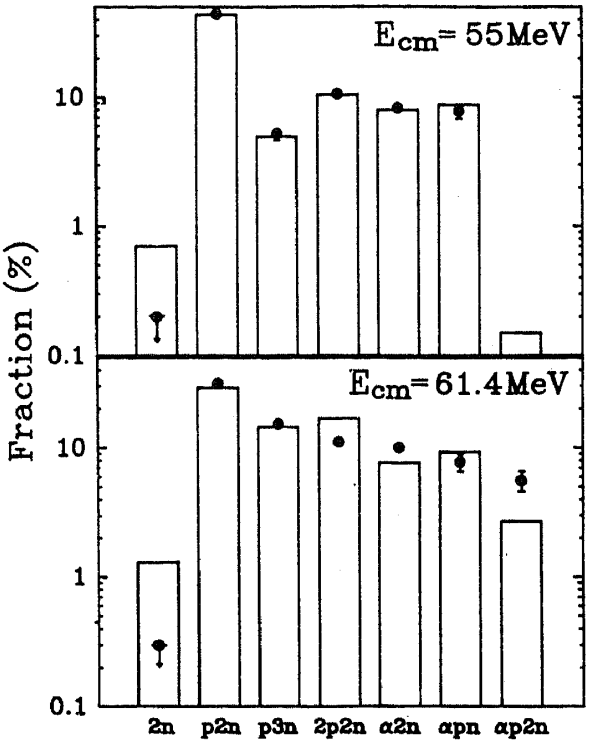

Figure 5. Detailed comparison between measured and calculated fractional evaporation residue yields in fusion reactions of $^{28}Si + ^{68}Zn$ at two different energies. The calculations were performed using the statistical model code CASCADE (see text).

energy for lighter nuclei i.e., for $A \sim 88$–90. However, since this channel is not more than $\sim 10\%$ of the total fusion cross-section for any of the measured cases, no fine tuning of the parameters was attempted to achieve a better fit to the data. Thus, a fairly good agreement between the CASCADE predictions and the major channels establishes the reliability of the parameters used in the code and these predictions could be used for further calculations of total fusion cross-section. Since the missing channels constitute only 15–25% of the total fusion cross-sections, the uncertainties in the derived fusion cross-sections due to uncertainties in the CASCADE parameters are small. An uncertainty of 20% on the estimation of the missing channels by CASCADE has been assumed to estimate the uncertainties in the total fusion cross-section. Tables 3 to 6 give the total cross-sections for the four systems calculated from the experimentally measured partial ER cross-sections as explained earlier.

4. Determination of average angular momenta

The relative cross-sections for different evaporation residues are dependent on the angular momentum distribution in the compound nucleus (Hass *et al* 1985). Figure 6 shows, for example, the fractional cross-section of $p2n$ and $(2p2n + p3n)$ channel as a function of angular momentum of the compound nucleus for a given excitation energy, as predicted by CASCADE. In practice, however, the compound nucleus is formed with a distribution in ℓ and the fractional cross-section of any ER has to be folded with the ℓ-distribution in the compound nucleus. Figure 7 shows the variation of

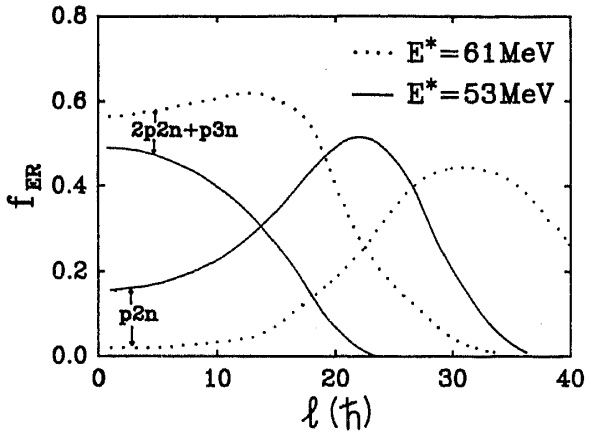

Figure 6. CASCADE predictions for the fractional cross-section for $p2n$ and $2p2n + p3n$ as a function of angular momentum, ℓ, in the compound nucleus for fixed excitation energy.

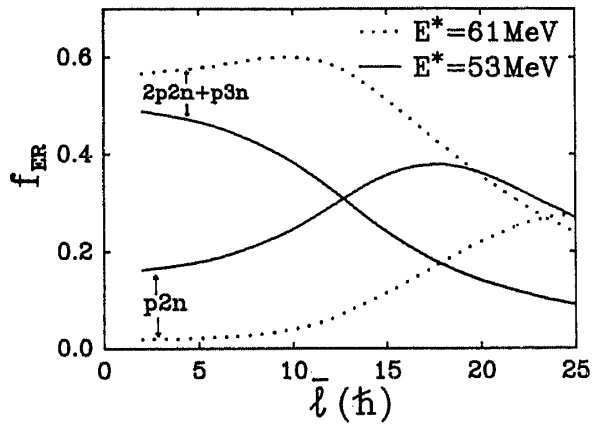

Figure 7. Same as figure 6 but as a function of average angular momentum ($\bar{\ell}$) in the compound nucleus.

partial ER cross-sections for $p2n$ and $(2p2n + p3n)$ channels as a function of average angular momentum for a fixed excitation energy of the CN. The average angular momentum is given by

$$\bar{\ell} = \frac{\sum_{\ell=0}^{\infty} \sigma_\ell \ell}{\sum_{\ell=0}^{\infty} \sigma_\ell}. \tag{5}$$

For these calculations, a Woods–Saxon form of ℓ-distribution, given by (4) with a diffuseness parameter of $a = 0{\cdot}06\ell_0$ was used. This value of the diffuseness parameter is estimated from the consideration that the ℓ-distribution at a given energy follows the impact parameter distribution, which in turn depends on the density distribution of the nucleus. Thus, one expects $(a/\ell_0) \simeq (a_n/R)$ where a_n is the diffuseness of the density distribution for a nucleus of radius R.

The figure clearly shows that an accurate measurement of partial ER cross-section or relative ER cross-sections can be used to determine average angular momentum of the CN. In the present work, this dependence has been exploited to get $\bar{\ell}$ of the

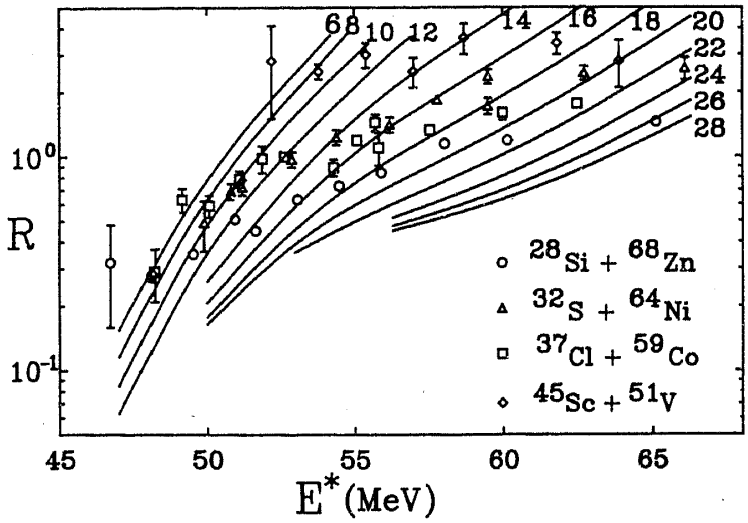

Figure 8. The ratio $R = \sigma_{p3n+2p2n}/\sigma_{p2n}$ as a function of the excitation energy in the compound nucleus ^{96}Ru. The four symbols represent the experimentally measured values for the four systems and the solid lines are the result of calculations with different $\bar{\ell}$ as described in the text. The $\bar{\ell}$ values are written alongside the curves.

CN. The relative evaporation residue cross-sections for $p2n$ and $(2p2n + p3n)$ channels were used for this purpose. These were chosen since they being the dominant channels in the energy range covered in this work, have the least error in the cross-section measurements.

The expected ratio R of the $(2p2n + p3n)$ to $p2n$ cross-sections from the statistical model calculations is plotted in figure 8, as a function of excitation energy in the CN for various values of ℓ_0 and hence $\bar{\ell}$. The experimentally measured values of R at the excitation energies corresponding to the bombarding energies at which the measurements were made are also shown in this figure. The $\bar{\ell}$'s were derived for the measured systems from a comparison of the experimental values of R and the calculated curves of figure 8. The $\bar{\ell}$ so obtained are given in tables 3–6 for all the four systems. The relation between the $\bar{\ell}$ and the fusion excitation function has been discussed in an earlier publication (Dasgupta *et al* 1991).

In the process of relating the $\bar{\ell}$ to the relative ER yields, two factors have been used as inputs viz the ℓ-distribution in the CN and the partial ER cross-sections as predicted by CASCADE, which in turn depends on the parameters of the code. Therefore a detailed investigation of the effects of ℓ-distribution and CASCADE parameters is essential in order to estimate the uncertainties in the $\bar{\ell}$ derived by such method.

4.1 *Sensitivity of $\bar{\ell}$ to the ℓ-distributions*

The sensitivity of the $\bar{\ell}$ to the assumed distribution was investigated in two ways. In the first, the effect of varying the width a in the distribution given by (4), keeping the $\bar{\ell}$ same were investigated. Next, different ℓ-distributions having same $\bar{\ell}$, but different shapes were considered. The ℓ-distributions considered are,

(i) a Gaussian distribution of the form,

$$\sigma(\ell) \propto \exp[-(\ell - \ell_0)^2/2a^2] \qquad (6)$$

with $a/\ell_0 = 0{\cdot}15$, $0{\cdot}3$ and $0{\cdot}45$;

(ii) a Woods–Saxon distribution given by (4) with $a/\ell_0 = 0{\cdot}04$, 0·06, and 0·08 and (iii) a flat distribution of $\sigma(\ell) =$ constant for $0 < \ell \leqslant 2\ell_0$ and 0 for $\ell > 2\ell_0$.

It was pointed out earlier, that for below and near barrier fusion reactions, the ℓ-distribution is known to become broader than triangular distributions. The flat-distribution assumed above, though unrealistic, is considered to represent the extreme form of the aforesaid observation. The $\bar{\ell}$'s derived for the measured systems from a comparison of the experimental values of fractional cross-sections of $p2n$, $2p2n + p3n$ and R and the calculated curves for these various distributions, are given in tables 8(a)–(c) for $^{28}Si + {}^{68}Zn$ system. The values derived from $p2n$, $2p2n + p3n$ and their ratios can be seen to be consistent till centre of mass energy of 63·6 MeV.

Table 8(a). Summary of the derived average angular momentum, $\bar{\ell}$, in units of $\hbar$, for distribution of the form (*A*) $\sigma(\ell) \propto (2\ell + 1)[1 + \exp\{(\ell - \ell_0)/a\}]^{-1}$ with $a/\ell_0 = 0{\cdot}03$, 0·06, 0·09 for $^{28}Si + {}^{68}Zn$ system. $\bar{\ell}$ derived from the partial cross-section in (i) $p2n$, (ii) $2p2n + p3n$ and (iii) $2p2n + p3n/p2n$ are given for $a/\ell_0 = 0{\cdot}06$. Uncertainties, quoted within brackets, include the error due to relative cross-section measurements only (see text).

E_{CM}	$a = 0{\cdot}06\ell_0$			$a = 0{\cdot}03\ell_0$	$a = 0{\cdot}09\ell_0$
(MeV)	(i)	(ii)	(iii)	(iii)	(iii)
52·2	< 6	< 6	< 6	< 6	< 6
53·6	6·0(4·0)	5·8(1·0)	6·2(0·8)	6·2(0·8)	6·2(0·8)
55·0	10·5(3·5)	9·8(1·8)	10·1(0·5)	10·1(0·5)	10·1(0·5)
56·4	13·7(1·7)	12·0(1·0)	12·4(0·4)	12·5(0·4)	12·2(0·6)
57·1	16·0(3·0)	14·4(1·0)	14·8(0·4)	14·8(0·4)	15·1(0·6)
58·6	16·0(1·2)	15·2(0·6)	15·4(0·4)	15·5(0·6)	16·0(0·6)
60·0	17·5(1·5)	17·8(0·6)	17·5(0·4)	17·3(0·4)	17·8(0·4)
61·4	18·0(1·0)	19·1(0·6)	18·5(0·4)	18·2(0·4)	18·9(0·4)
63·6	18·0(1·0)	20·0(0·6)	19·1(0·4)	19·0(0·4)	19·5(0·4)
65·7	18·6(0·6)	24·0(1·6)	21·4(1·3)	21·0(0·4)	21·5(0·5)
70·7	22·1(0·8)	31·5(1·0)	26·5(0·5)	26·0(0·5)	26·7(0·4)

Table 8(b). Same as table (8a) but for a distribution of the form $\sigma(\ell) \propto \exp[-(\ell - \ell_0)^2/2a^2]$ with $a/\ell_0 = 0{\cdot}15$, 0·30, 0·45.

E_{CM}	$a = 0{\cdot}3\ell_0$			$a = 0{\cdot}45\ell_0$	$a = 0{\cdot}15\ell_0$
(MeV)	(i)	(ii)	(iii)	(iii)	(iii)
52·2	< 6	< 6	< 6	< 6	< 6
53·6	6–18	6·0(0·7)	6·3(0·7)	6·2(0·5)	6·6(0·8)
55·0	10–20	9·8(1·2)	10·5(0·5)	10·3(0·6)	10·5(0·5)
56·4	13–22	12·6(0·8)	12·7(0·5)	12·5(0·5)	12·8(0·4)
57·1	13–22	13·8(0·8)	14·6(0·6)	14·8(0·5)	14·4(0·3)
58·6	14–24	15·6(0·5)	16·0(0·5)	16·3(0·6)	15·9(0·3)
60·0	14–26	17·5(0·5)	17·6(0·6)	18·2(0·6)	17·4(0·4)
61·4	16–28	19·3(0·6)	18·9(0·6)	19·6(0·5)	18·8(0·3)
63·6	19·0(0·5)	20·6(0·8)	19·8(0·4)	20·0(0·4)	19·8(0·3)
65·7	19·5(0·5)	24·0(0·8)	22·0(0·5)	23·0(0·7)	22·0(0·3)
70·7	22·5(1·0)	31·4(0·6)	27·3(0·5)	28·8(0·5)	26·8(0·3)

Table 8(c). Same as table 8(a) but for a flat distribution of the form, $\sigma(\ell)$ = constant for $0 < \ell \leqslant 2\ell_0$ and 0 for $\ell > 2\ell_0$.

E_{CM}(MeV)	(i)	(ii)	(iii)
52·2	< 4	< 8	< 5
53·6	< 8	6·0(1·8)	5·2(0·4)
55·0	10(2)	10·0(1·0)	9·7(0·2)
56·4	> 14	12·1(1·0)	12·8(0·6)
57·1	> 14	15·4(0·8)	> 18
58·6	> 14	16·2(1·0)	> 18
60·0	> 14	18·6(1·7)	> 18
61·4	> 14	21·2(0·8)	> 18
63·6	> 16	20·9(1·7)	> 18
65·7	16–22	24·8(1·0)	> 18
70·7	> 18	26·0(1·0)	> 18

However, for flat ℓ-distribution, the $\bar{\ell}$ becomes insensitive to the fractional $p2n$ cross-section and R. Similarly for a Gaussian distribution, the $\bar{\ell}$ becomes insensitive to the fractional cross-section for $p2n$. At higher energies, the $\bar{\ell}$ derived from fractional cross-sections for $p2n$, $2p2n + p3n$ and their ratio R are not consistent with each other. The $\bar{\ell}$ derived from the fractional cross-section for $p2n$ channel is lower than those derived from $2p2n + p3n$ channel. Such a comparison shows that a $\bar{\ell}$ can be derived within an uncertainty of $\pm 1\,\hbar$ for energies up to 63 MeV and $\pm 5\,\hbar$ for higher energies. The changes in the derived $\bar{\ell}$ for the various ℓ-distributions listed above are $\sim 0{\cdot}5$ to $1{\cdot}0\,\hbar$ for $4\,\hbar \leqslant \bar{\ell} \leqslant 8\,\hbar$, $\sim 0{\cdot}5\,\hbar$ for $8\,\hbar \leqslant \bar{\ell} \leqslant 20\,\hbar$ and 1 to $2\,\hbar$ for $\bar{\ell} > 20\,\hbar$. The relative insensitivity of the fractional cross-sections to the different ℓ-distributions with the same $\bar{\ell}$ results when one considers major decay channels which are not near a threshold. For such channels, the partial cross-sections do not vary very sharply with ℓ in the relevant region. The sensitivity to higher moments of ℓ is greater.

4.2 *Sensitivity of $\bar{\ell}$ to the CASCADE parameters*

In order to check the variation of $\bar{\ell}$ with the parameters in the statistical model code CASCADE, the level density parameter, the backshifting parameter and the diffuseness parameter d_α in the real part of the WS potential [for the calculation of the α-transmission coefficients] were varied. The other parameters in the code viz., the ground state masses, pairing energy and the moment of inertia parameter were not varied as these were obtained from experimentally determined quantities. Variation of the γ-decay strength within reasonable limits is not expected to change the relative ER yields significantly.

(i) *Level density parameter*: The effect of changing the level density parameter was investigated by keeping all the other parameters fixed (ℓ-distribution of the form given by 4, no backshifting of the ground state, $d_\alpha = 0{\cdot}58$ fm) and then varying the level density parameter from $A/8$ to $A/10$. The effect of changing the level density parameter on the $\bar{\ell}$ is shown in figure 9. It is seen to change the derived $\bar{\ell}$ values by $\pm 2\,\hbar$ units. However, it is seen that a variation of level density parameter beyond $A/8{\cdot}5$ to $A/9{\cdot}5$ does not give consistent values for $\bar{\ell}$ when all the channels are included. Thus, a

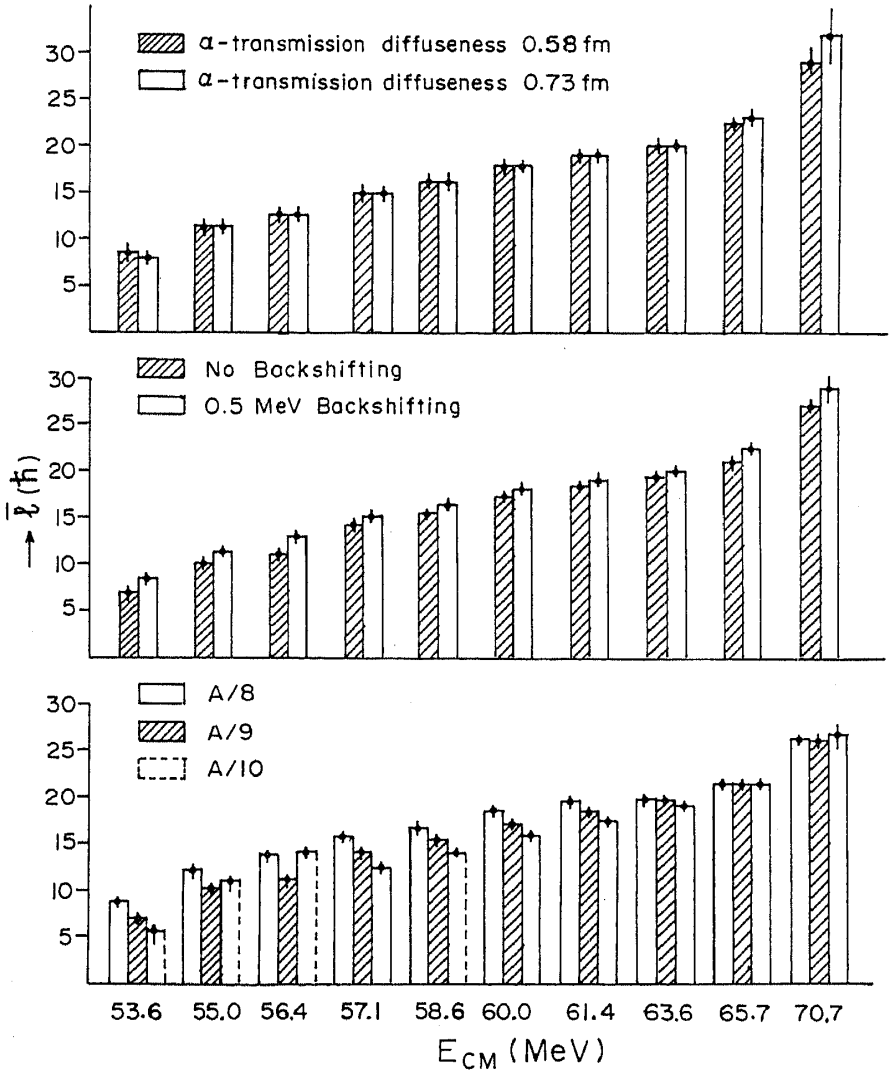

Figure 9. Sensitivity of the derived average angular momentum ($\bar{\ell}$) on the various CASCADE parameters (see text). The figure shows the derived $\bar{\ell}$ for the case of $^{28}Si + {}^{68}Zn$.

variation of level density parameter within a reasonable limit of $A/8{\cdot}5$ to $A/9{\cdot}5$ changes the derived $\bar{\ell}$ by $\pm 1\,\hbar$.

(ii) The backshifting parameter: The effect of changing the backshifting parameter was investigated by keeping all the other parameters fixed (ℓ-distribution of the form given by 4, level density parameter $A/9$, $d_\alpha = 0{\cdot}58$ fm) and then varying the backshifting parameter such that there is in one case no shift of the ground state while for the other case the ground state is shifted by 0·5 MeV (as prescribed by Dilg *et al* 1973). The effect of this variation on the $\bar{\ell}$ is shown in figure 9. It is seen to introduce a variation of 1–2 ħ units at the lower ($E^* \leqslant 52$ MeV) and higher energy ($E^* \geqslant 61$ MeV) regions.

(iii) The α-potential diffuseness [d_α] for the calculation of the α-transmission coefficients: The effect of changing d_α was investigated by keeping all the other parameters fixed (ℓ-distribution of the form given by 4, level density parameter $A/9$, ground state backshifted by 0·5 MeV) and then varying the d_α from 0·58 fm to 0·73 fm. The effect of this variation on the $\bar{\ell}$ is shown in figure 9. The parameter d_α does not seem to affect the derived $\bar{\ell}$ within the experimental uncertainties.

Thus detailed comparisons with such variation of the parameters show that $\bar{\ell}$ can be reliably obtained to within an uncertainty of 1 ħ to 2 ħ for $\bar{\ell}$ values not exceeding 20 ħ by using the fractional cross-sections of $p2n$, $p3n$ and $2p2n$ channels.

5. Summary and discussion

It is shown that a good agreement can be achieved between the experimental and calculated branching ratios for the decay of the CN ^{96}Ru for a consistent set of statistical model parameters. With this agreement, a method is suggested where these ratios can be used to determine the average angular momentum in fusion reactions. There are several previously known methods for determining various moments of angular momentum distribution, viz., γ-ray multiplicity measurements, fission fragment angular distribution, particle angular distribution and correlation, and isomer ratios. This method of finding $\bar{\ell}$ can be compared with the other methods of determining $\bar{\ell}$ in the cases where both ER measurements as well as $\bar{\ell}$ values determined by other methods are available. In the case of $^{16}O + ^{154}Sm$ partial cross-sections (Stokstad *et al* 1980) for $3n, 4n$ and $5n$ channels as well as $\bar{\ell}$ determined from γ-multiplicity measurements (Vandenbosch *et al* 1983) have been reported. It would be interesting to compare the $\bar{\ell}$ values determined by the method used in the present work and the γ-ray multiplicity measurements. The parameters used (see §3.1) in the code CASCADE were fixed by comparison of the relative ER yields for $3n$ and $4n$ channels at above barrier energies. Having fixed the CASCADE parameters, the $\bar{\ell}$ values were obtained using the method explained in §4. Cross-sections for $3n$ and $4n$ channels and a Woods–Saxon form of the ℓ-distribution given by (4) were used to determine $\bar{\ell}$ values. The $\bar{\ell}$ values so derived are found to agree with those reported from the γ-multiplicity measurements. The values are plotted in figure 10. The $\bar{\ell}$ values obtained using a Woods–Saxon ℓ-distribution in the CN agrees with those obtained using a flat distribution within the experimental uncertainties. This observation again points to the relative insensitivity of the fractional cross-sections for the major decay channels to the ℓ-distribution. The $\bar{\ell}$ values reported by Vandenbosch *et al* (1983) are also plotted in figure 10. It can be seen that $\bar{\ell}$ values obtained by the present method

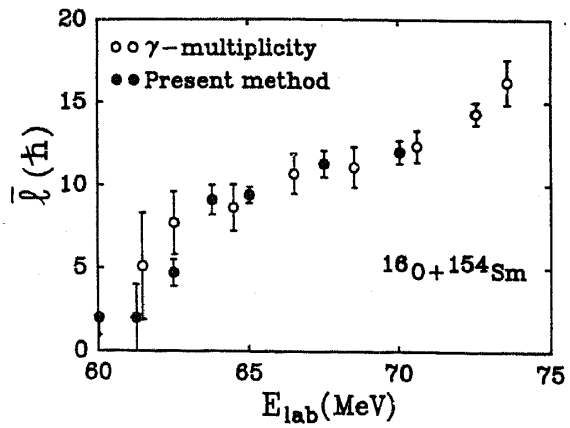

Figure 10. Comparison of average angular momentum ($\bar{\ell}$) derived using (**a**) the present method and (**b**) from gamma multiplicity measurements of Vandenbosch *et al* (1983) for the $^{16}O + ^{154}Sm$ system.

agrees fairly well with those derived from γ-multiplicity measurements. However, the agreement between the $\bar{\ell}$ values determined by these two methods for lower values of excitation energies is not good. This is attributed to the fact that the CASCADE predictions for the relative ER yields, with the set of parameters used, do not match very well with the experimental values for channels which are near threshold. A finer tuning of the parameters, than what is attempted here, may be required to achieve such an agreement.

In summary, we have measured the ER cross-section following fusion reactions of $^{28}Si + {}^{68}Zn$, $^{32}S + {}^{64}Ni$, $^{37}Cl + {}^{59}Co$ and $^{45}Sc + {}^{51}V$ for centre of mass energies ~ 5 MeV below to ~ 10 MeV above the Coulomb barrier. We find that for each of the four different entrance channel combinations fairly good agreement is found between the statistical model predictions and the experimental partial cross-sections with one set of statistical model parameters. Thus, for the CN ^{96}Ru formed near the Coulomb barrier no significant entrance channel effect is found on the decay mode. It is shown that the average angular momentum in fusion reactions can be determined from a measurement of the fractional cross-section of the evaporation residues. The sensitivity of the determined average angular momentum on the various statistical model parameters have been investigated and it is found to yield the value of $\bar{\ell}$ within an uncertainty 1–2 $\hbar$. In the case of $^{16}O + {}^{154}Sm$, the $\bar{\ell}$ deduced by this method agrees with those determined by γ-multiplicity measurements, establishing the validity of this technique.

Acknowledgements

We wish to thank D C Ephraim and A R Pednekar for their help in target preparation, S Chattopadhyay for help during the experiments and the pelletron accelerator staff for their co-operation during the runs. We gratefully acknowledge useful discussions with D R Chakravarty, V M Datar and S Kailas.

References

Ajzenberg-Selove F 1986 *Nucl. Phys.* **A449** 1
Alexander J M, Guerreau D and Vaz L C 1982 *Z. Phys.* **A305** 313
Beckerman M 1988 *Rep. Prog. Phys.* **51** 1047
Dasgupta M, Navin A, Agarwal Y K, Baba C V K, Jain H C, Jhingan M L and Roy A 1988 *Proc. DAE Symp. Nucl. Phys.* Bombay, India **B31** O-18
Dasgupta M, Navin A, Agarwal Y K, Baha C V K, Jain H C, Jhingan M L and Roy A 1991 *Phys. Rev. Lett.* **66** 1414
Dilg W, Schantl W, Vonach H and Uhl M 1973 *Nucl. Phys.* **A217** 269
Fernández-Niello J, Dasso C H and Landowne S 1989 *Comp. Phys. Commun.* **54** 409
Grover J R and Gilat J 1967 *Phys. Rev.* **157** 802
Hass B *et al* 1985 *Phys. Rev. Lett.* **54** 398
Huizenga J R and Igo G 1961 *Nucl. Phys.* **29** 242
Lederer C M and Shirley V S 1978 *Table of Isotopes* Seventh edn (New York: John Wiley)
Mosel U 1985 in *Treatise on heavy ion science* (ed.) D A Bromley (New York and London: Plenum Press) Vol. 2 p. 3
Navin A, Dasgupta M, Baba C V K and Roy A 1989 *Proc. of DAE Symp. Nucl. Phys.* Aligarh, India **B32** P 59
Northcliffe L C and Schilling R F 1970 *Nucl. Data Tables* **A7** 233
Perey F G 1963 *Phys. Rev.* **131** 745

Pühlhofer F 1977 *Nucl. Phys.* **A280** 267
Ruckelshausen A *et al* 1986 *Phys. Rev. Lett.* **56** 2356
Sarantities D G and Pakes B D 1967 *Nucl. Phys.* **A93** 545
Signorini C, Skorka S, Spolaore P, Vitturi A (eds) 1988 *Proceedings of the International symposium on heavy ion interactions around the coulomb barrier*, Legnaro (Italy) (Springer, Berlin, 1988)
Steadman S G and Rhoades-Brown M J 1986 *Annu. Rev. Nucl. Part. Sci.* **36** 649
Stokstad R G, Eisen Y, Kaplanis S, Pelte D, Smilansky U and Tserruya I 1980 *Phys. Rev.* **C21** 2427
Thomas T D 1964 *Nucl. Phys.* **53** 558
Vandenbosch R, Back B B, Gil S, Lazzarini A and Ray A 1983 *Phys. Rev.* **C28** 1161
Wapstra A H and Bos K 1977 *At. Nucl. Data Tables.* **19** 175
Wilmore D and Hodgson P E 1964 *Nucl. Phys.* **55** 673

Note added in proof

Gil *et al* (1991 *Phys. Rev.* **C43** 701) have recently reported $\bar{\ell}$ values for $^{16}O + ^{154}Sm$ system using γ-ray multiplicity measurements. These $\bar{\ell}$ values are generally larger by 2–4 $\hbar$ units as compared to those reported by Vandenbosch *et al* (1983). The $\bar{\ell}$ values obtained using the method suggested in the present work shown in figure 10 are calculated using a value of $A/9$ for the level density parameter. If instead a value of $A/8$ is used the derived $\bar{\ell}$ values increase by 3–4 $\hbar$ units and are generally found to agree with the recent results of Gil *et al* (1991). The present method of deriving $\bar{\ell}$ is expected to work well when the change in the level density brought about by including the rotational energy $\ell(\ell+1)\hbar^2/2I$ is comparable or larger than that due to changes in the statistical model parameters, e.g. a. This implies that the present method is expected to be good for higher ranges of $\bar{\ell}$ as the mass number of the compound nucleus increases. The authors wish to thank S Kailas for bringing the reference (Gil *et al*) to their notice.